Chemical Engineering & Processing: Process Intensification 199 (2024) 109734

Contents lists available at ScienceDirect

Chemical Engineering and Processing - Process Intensification

journal homepage: www.elsevier.com/locate/cep

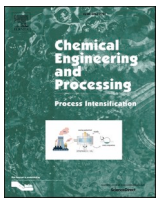

# Intensification of evaporative precipitation of lignin in a spinning disc evaporator

Thomas Carr, Fernando Russo Abegão, Kamelia Boodhoo *

*School of Engineering, Faculty of Science, Agriculture and Engineering, Newcastle University, Newcastle upon Tyne NE1 7RU, UK*

ARTICLE INFO

*Keywords:*
Process intensification
Spinning disc
Evaporative precipitation
Lignin
Organosolv black liquor

ABSTRACT

A continuous process for the evaporative precipitation of lignin derived from Organosolv black liquor was successfully developed and implemented in a spinning disc evaporator (SDE). A maximum of 95 % of the lignin was recovered at a disc speed of 1200 rpm, black liquor feed flow rate of 1 ml $s^{-1}$ on a smooth disc surface heated to 100 °C. These optimal flow rate and disc speed values corresponded to conditions which maximised residence time to <1 s in 4 disc passes without compromising on the rate of evaporative heat transfer. The lignin precipitate did not have any detectable impurities present after being washed and dried. The particle size for the lignin precipitate was in the region of 3 – 9 μm with minor agglomeration occurring, providing good filterability. A scaled up version of the process was modelled for benchmarking purposes and it was found that the SDE had a better theoretical performance than a falling film evaporator (FFE) system developed for the same process, with the energy consumption reduced by 23% and a higher lignin recovery rate per volume of black liquid processed once adjusted for processing time (38.1 g $L^{-1}$ $h^{-1}$ for the SDE *vs.* 3.23 g $L^{-1}$ $h^{-1}$ for the FFE).

## 1. Introduction

Due to increasing global population and the need for more sustainable methods to maintain standards of living, there has been increasing demands for biobased renewable chemicals to replace fossil-based derivatives. Lignocellulosic biomass is the type of biomass with the largest global availability, with over 100 million tonnes attainable for sustainable use in Europe per year [1] making it an ideal resource to exploit for a bioeconomy. It has a low cost and is rich in cellulose and hemicellulose, the two most abundant polysaccharides on earth [1]. It also contains lignin, the second most profuse biopolymer after cellulose [2].

Lignin is currently separated from cellulose in the pulping industry, using several processes based on the Kraft, Soda, Organosolv and Sulphite techniques [3,4]. Organosolv lignin has been found to be of the highest quality, with regards to purity, sulphur and ash content, homogeneity, increased syringyl phenolic units and condensed phenolic structures [5,6]. The black liquor (BL) produced from the pulping step in the Organosolv process consists mainly of ethanol and water, containing the dissolved lignin and partially hydrolysed hemicellulose sugars. Therefore, it has the potential to act as a "green crude" in a biorefinery, where lignin can be converted into a biorenewable feedstock for multiple products, including phenols, aromatics, fuels, polymers and carbon fibres [2,7,8]. Nevertheless, 98 % of the approximately 50 million tonnes of lignin produced annually are incinerated to produce energy, due to its complex structure and costs associated with producing a pure product [10]. Furthermore, lignin acts as a barrier to the hydrolysis of sugars [9] and it must be removed from this upstream biorefinery stream in order to enable effective conversion of the hemicellulose sugars downstream.

Effective separation of lignin is vital for an economically and environmentally sustainable biorefinery. Previous methods of removing lignin from pulping liquors involved diluting BL with an antisolvent (usually water) [11–14], membrane filtration [15] or solvent evaporation [5]. Antisolvent dilution works by increasing supersaturation via addition of suitable chemical, *i.e.* the antisolvent, which is miscible with the bulk solution, but which greatly reduces lignin solubility. Through this method, lignin recoveries just under 75 % can be achieved [11]. However, the volume of filtrate is dramatically increased, making it challenging and costly to recycle the antisolvent and process the overly diluted hemicellulose downstream. It also creates lignin with poor filtration properties due to typically small particle sizes (0.5 – 2.5 μm) [16], making the antisolvent technique challenging for optimal biorefinery operation. Membrane filtration provides an alternative process route, but it struggles to effectively separate the lignin from the hemicellulose [17] and suffers from fouling [18] making it a less desirable

* Corresponding author.
*E-mail address:* kamelia.boodhoo@newcastle.ac.uk (K. Boodhoo).

https://doi.org/10.1016/j.cep.2024.109734
Received 1 December 2023; Received in revised form 2 February 2024; Accepted 29 February 2024
Available online 7 March 2024

**Nomenclature**

*Acronyms*

| | |
|---|---|
| 5-HMF | 5-hydromethylfufural |
| ATR - FTIR | Attenuated Total Reflection - Fourier Transform Infrared Spectroscopy |
| BL | Black Liquor |
| CSTR | Continuous Stirred Tank Reactor |
| DSC | Differential Scanning Calorimetry |
| FFE | Falling Film Evaporator |
| FhG | Fraunhofer Centre for Chemical-Biotechnological Processes |
| HPLC | High Pressure Liquid Chromatography |
| PBL | Processed Black Liquor |
| SDE | Spinning Disc Evaporator |

*Notation*

| | |
|---|---|
| $A$ | Disc surface area, $m^2$ |
| $c_p$ | Specific heat capacity, J $kg^{-1}$ $K^{-1}$ |
| $d_e$ | Equivalent hydraulic diameter, m |
| $h$ | Film heat transfer coefficient, W $m^{-2}$ $K^{-1}$ |
| $j_h$ | Heat-transfer factor ($=0.023\ Re^{-0.2}$) |
| $k$ | Thermal conductivity, W $m^{-1}$ $K^{-1}$ |
| $m_{BL,Sample}$ | Mass of black liquor solution used for initial lignin content determination, kg |
| $m_{BLTotal}$ | Initial mass of unprocessed black liquor fed into the SDE, kg |
| $m_{Lig,BLsample}$ | Mass of dried lignin precipitate, kg |
| $m_{Lig,BLTotal}$ | Mass of lignin in the total volume of initial unprocessed BL, kg |
| $m_{Lig,PBL}$ | Mass of lignin precipitated from the PBL supernatant sample, kg |
| $m_{Lig,PBLTotal}$ | Mass of lignin dissolved in the concentrated black liquor after 4 passes through the SDE, kg |
| $m_{Lig,pp}$ | Total mass of lignin precipitated after 4 passes in the SDE, kg |
| $m_{PBL,Sample}$ | Mass of supernatant sample taken, kg |
| $m_{PBLTotal}$ | Mass of concentrated black liquor after 4 passes through the SDE, kg |
| $N$ | Disc speed, rpm |
| $Pr$ | Prandtl number ($\frac{\mu^* c_p}{k}$) |
| $q$ | Heat transfer rate, W |
| $Q$ | Flow rate, $m^3$ $s^{-1}$ |
| $r$ | Radius, m |
| $R_{Lig}$ | Lignin recovery, % |
| $Re$ | Reynolds number ($\frac{2Q\rho}{\pi\mu r}$) |
| $Sc$ | Schmidt number ($\frac{\nu}{D}$) |
| $T$ | Temperature, K |
| $\Delta T_{lm}$ | Logarithmic mean temperature difference, K |
| $T_g$ | Glass transition temperature, K |
| $t_{res}$ | Residence time, s |
| $u$ | Average radial velocity of thin film, m $s^{-1}$ |
| $U$ | Overall heat transfer coefficient, W $m^{-2}$ $K^{-1}$ |
| $V$ | Volume, $m^3$ |
| $w_{Lig,BL}$ | Initial mass fraction of lignin in unprocessed black liquor |
| $w_{Lig,PBL}$ | Mass fraction of lignin remaining in black liquor after 4 passes through SDE |

*Greek symbols*

| | |
|---|---|
| $\gamma$ | Shear rate, $s^{-1}$ |
| $\delta$ | Film thickness, m |
| $\mu$ | Dynamic viscosity, N s $m^{-2}$ |
| $\nu$ | Kinematic viscosity, $m^2$ $s^{-1}$ |
| $\rho$ | Density, kg $m^{-3}$ |
| $\omega$ | Angular speed, rad $s^{-1}$ |

*Subscripts*

| | |
|---|---|
| i | Inner |
| o | Outer |

technique when the content of lignin to remove is high.

As lignin is soluble in ethanol, but insoluble in water, and ethanol is more volatile than water, evaporative precipitation via removal of the ethanol solvent is an effective method of precipitating lignin from ethanolic Organosolv BL. Not only does the process recover ethanol for reuse in the biorefinery, as the concentrated stream also facilitates downstream hemicellulose processing. However, current methods utilising continuous stirred tank reactors and falling film evaporators have high energy and long processing time requirements [5]. Lignin precipitation via solvent evaporation can also form encrustations on the equipment surfaces, reducing their performance and lowering lignin yields.

There is scope for intensified process technologies to further improve evaporative precipitation and crystallisation techniques, especially by enhancing the heat transfer in the process and reducing the energy consumption required to volatilise the solvent. One method to achieve this is by using mechanical vapor recompression (MVR), where the vapor generated during evaporation is mechanically compressed, and then used to provide heat for the evaporation process. This reduces the heating duty of the boiler energy requirements and operating costs. This method has been successfully applied on a wide range of applications, from radioactive wastewater treatment (where the energy saving is as high as 88.7 % compared with the traditional evaporator) [19] to crystallising bittern [20]. Microwaves have also been used to accelerate glycine crystallisation. The use of microwaves and silver particles decreased crystallisation time approximately 60 times when compared to the conventional evaporative crystallisation technologies [21]. This is a consequence of the microwaves rapidly causing a temperature gradient between the solvent and the nanostructured particles, which accelerates mass transfer, and thereby, nucleation.

The spinning disc evaporator (SDE) has been identified as a promising technology to intensify the evaporative precipitation of lignin. Due to centrifugal forces generated by the spinning action, a stable thin film is produced on the surface of the spinning disc with a short diffusional path length, enabling rapid mixing and heat transfer [22,23]. The high surface area to volume ratio offered by the wavy thin film (typically in the region of $10^4$ $m^2/m^3$ even in large scale devices [22]) has the potential to enhance the rates of heat transfer into the liquid and of mass transfer at the liquid-vapour interface [24,25], resulting in shorter processing time required to achieve a desired level of supersaturation and precipitation. The near plug flow characteristics [26] ensure that the residence time distribution is tightly controlled so that the products experience near identical processing conditions for uniformity in product properties such as particle size distribution. Whilst the spinning disc technology has previously been successfully utilised to intensify precipitation processes in earlier work [26,27,28,29], there is a lack of research on applications of the technology to evaporative precipitation. Therefore, precipitating lignin from a lignocellulosic hydrolysate stream via solvent evaporation is a novel application of the spinning disc technology.

This paper presents the development of an intensified method for continuous lignin precipitation using a SDE system to create thin films

under high shear conditions, leading to mixing and heat and mass transfer intensification in the solvent evaporation process. Optimal SDE processing conditions that maximise lignin yield, purity and particle size were also investigated, in order to facilitate integration, implementation and scale up of the processes for use in a full scale biorefinery.

## 2. Materials

The black liquor (BL) was kindly provided by Fraunhofer CBP as part of the EU H2020 BBI JU BioSPRINT project. The BL was produced by the Organosolv process at Fraunhofer CBP's lignocellulose biorefinery pilot plant. The BL production was not an integral part of this study, with the process and conditions for generating the Organosolv BL from hardwood described by Schulze [5]. The black liquor contained 43 %(w/w) ethanol, 1.5 %(w/w) lignin, 1 %(w/w) hemicellulose sugars, 0.5 %(w/w) acetic acid and 0.5 %(w/w) sulphuric acid. The balance being water with trace amounts of alkanes, furfural, esters, phenolics and other species solubilised during the pulping process. Organosolv lignin was provided by FhG and BioPiva 395 Kraft lignin from UPM was used for benchmarking purposes.

For quantification of sugars in solutions and precipitates, solutions of the sugar recovery standards were prepared using 98 % cellobiose, 99 % rhamnose, 99 % arabinose, 99 % mannose, 98 % galactose, 99 % fructose, 99 % xylose (all from Acros Organics) and 99 % glucose (Fisher Chemicals). 99.8 % analytical reagent grade ethanol (Fisher Chemicals) was used to create the calibration column used for ethanol concentration. HPLC water (Fisher Chemicals) was used in HPLC analysis. >95 %(w/w) analytical grade sulphuric acid (Fisher Chemicals) was utilised when acidified water was required for analysis.

## 3. Methods

### 3.1. Experimental equipment and procedure

A schematic of the overall SDE set up is presented in Fig. 1. The key equipment dimensions and processing conditions are detailed in Table 1. The SDE consisted of a 316 stainless steel disc encased in a stainless-steel evaporator housing. Two types of disc surfaces (grooved and smooth) were tested (Fig. 2).

The BL was preheated to 80 °C (just below its boiling point of 82.8 °C at atmospheric pressure) on a temperature-controlled hotplate prior to being pumped into the SDE via a Watson Marlow 323 peristaltic pump through a section of 4.7 mm internal diameter Viton tubing connected to ¼" stainless steel tubing. The underside of the disc surface was heated by recirculating Therminol SP heat transfer oil through the rotating shaft from a Grant LTD6 oil bath. The temperature of the disc was regulated during the process by feedback control via measurement from a type K thermocouple located at the centre of the underside surface of the disc. To prevent condensation of vapours inside the evaporator, the SDE lid

**Table 1**
Equipment dimensions and processing conditions for the evaporative precipitation of lignin.

| | |
|---|---|
| **Equipment Dimensions** | |
| Disc diameter | 100 mm |
| SDE feed tube inner diameter | 1.5 mm |
| Feed tube position above spinning disc | 10 mm |
| **Processing Conditions** | |
| Passes through the disc | 4 |
| Volume of BL processed per run | 0.5 L |
| Disc temperature | 100 °C |
| Nitrogen preheat temperature | 100 °C |
| Nitrogen flow rate | 2 L $min^{-1}$ |

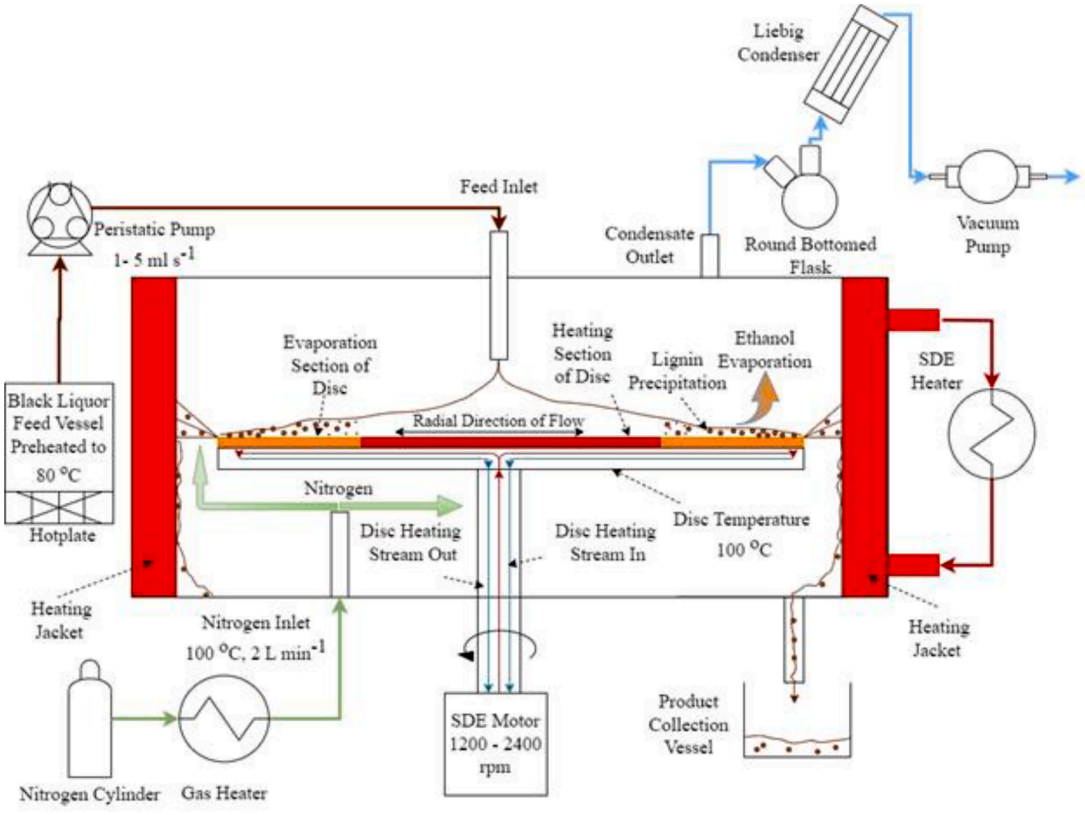


**Fig. 1.** Schematic of the evaporative precipitation of lignin set-up.

**Fig. 2.** Grooved and smooth discs used in the SDE.

was heated by electric heating pads whilst the SDE housing used heating oil. A hot nitrogen purge was used to aid the removal of solvent vapours formed during the evaporative process. Trace heating of the ¼" transfer line to the SDE was used to keep the BL at 80 °C. Lagging was placed around the SDE, SDE lid, feed vessel and transfer line to minimise heat loses throughout the system.

The processed BL leaving the SDE was transferred through an outlet pipe at the base of the evaporator into an ice-cooled vessel to ensure that evaporation only occurred within the housing. Samples were collected from the outlet pipe using a 3-way valve for analysis after each pass of the BL through the SDE. A maximum of 4 disc passes were implemented for each set of operating conditions, with ethanol removal and lignin recovery monitored after every pass. The evaporated solvent was removed through the lid of the SDE using a KNF Neuberger Laboport vacuum pump, with condensate samples collected in a round bottomed flask positioned under a Liebig condenser (jacket length 400 mm, internal diameter 25 mm), cooled to −15 °C using an ethylene glycol/water mixture in a Huber CC2 refrigeration bath circulator.

### 3.2. Design of experiments

Previous studies involving the evaporative precipitation of lignin in a falling film evaporator [5] and using a spinning disc reactor for $TiO_2$ reactive precipitation [26] found that product recovery is influenced by temperature, ethanol content, flow rate, disc rotational speed and disc surface configuration. A preliminary screening design was conducted to investigate the effect of disc speed (600 – 2400 rpm), feed flow rate (1 – 5 ml $s^{-1}$), and disc temperature (85 – 95 °C). The screening design indicated that flow rate and temperature were the most impactful parameters for lignin recovery and that higher disc speeds tended to favour greater lignin recovery. This informed the design of the full factorial optimisation study discussed in this work, performed using the variables outlined in Table 2 at a fixed disc temperature of 100 °C. This temperature was decided upon to the maximise the thermal driving force for solvent evaporation without the risk of sugar hydrolysis or dehydration occurring on the disc. This enabled the study to focus upon the optimisation of the SDE operating conditions. The impact of temperature and flow rate of the nitrogen purge was not investigated as existing literature indicates that the mass transfer rate for evaporative systems is limited by the liquid phase [30], so increasing the stripping effect would have minimal impact on the system.

**Table 2**
Processing conditions investigated in optimisation study.

| Variable | Levels | | |
|---|---|---|---|
| Disc surface | Smooth | Grooved | |
| Rotational speed / rpm | 1200 | 1800 | 2400 |
| Flow rate / ml $s^{-1}$ | 1 | 2.5 | 5 |

To benchmark the data, a comparison was made with data provided by the Fraunhofer Centre for Chemical-Biotechnological Processes using a falling film evaporator.

### 3.3. Product yield

#### 3.3.1. Gravimetric analysis

The yield of lignin precipitated in the SDE was determined in relation to the total content of lignin that was precipitable from the unprocessed black liquor (BL). Additionally, the mass balance was carried out indirectly with the soluble lignin fractions and liquid volumes, rather than using the precipitated lignin solids masses directly, as these solids could more easily deposit alongside the flow loops reducing the accuracy of the analysis.

Firstly, the mass fraction of lignin in the unprocessed BL, $w_{Lig,BL,}$ was determined gravimetrically. For this purpose, 15 ml of BL was weighed in a centrifuge tube, $m_{BLSample}$, to which 30 ml of acidified water (pH 2.1 acidified with 95 %(w/w) sulfuric acid) was added, causing the lignin to precipitate from solution. This was left in a fridge overnight before being centrifuged at 3500 ×*g* for 10 min on a SciSpin One. The supernatant was decanted and the lignin dried in a Jeio tech OV-11 oven at 40 °C and 500 mbar using a Vacuubrand PC 3001 Variopro vacuum pump. The dried lignin solids were weighed ($m_{Lig,BLSample}$) and a lignin mass fraction for the unprocessed black liquor, $w_{Lig,BL}$, was calculated from Eq. (1):

$$w_{Lig,BL} = \left(\frac{m_{Lig,BLSample}}{m_{BLSample}}\right) \times 100 \quad (1)$$

For the second step, it was necessary to determine the mass fraction of lignin that remained dissolved in the processed BL (PBL) after 4 passes through the SDE, $w_{Lig,PBL}$. Samples were taken from the product outlet after 4 passes through the SDE and allowed to cool to room temperature. The samples were then centrifuged for 10 min at 3500 ×*g* to remove the lignin precipitated in the SDE, and the supernatant was decanted, leaving any precipitate behind. Samples were taken from the supernatant fraction and weighed, $m_{PBLSample}$. Any lignin remaining in the supernatant was then precipitated with acidified water, centrifuged and dried using the same method outlined above. The mass of lignin precipitated from the PBL supernatant sample, $m_{Lig,PBL}$ was determined and the mass fraction of lignin that remained dissolved in the PBL after 4 passes through the SDE, $w_{Lig,PBL,}$ was calculated from Eq. (2):

$$w_{Lig,PBL} = \left(\frac{m_{Lig,PBL}}{m_{PBLSample}}\right) \times 100 \quad (2)$$

The mass of lignin in the total volume of initial unprocessed BL, $m_{Lig,BLTotal}$, and the total mass of lignin dissolved in the processed black liquor concentrated by evaporation after 4 passes through the SDE, $m_{Lig,PBLTotal}$ could then be determined using Eqs. (3) and 4, where $m_{BLTotal}$ is the initial mass of unprocessed black liquor fed into the SDE and $m_{PBLTotal}$ is the mass of concentrated black liquor after 4 passes through the SDE:

$$m_{Lig,BLTotal} = w_{Lig,BL} \times m_{BLTotal} \quad (3)$$

$$m_{Lig,PBLTotal} = w_{Lig,PBL} \times m_{PBLTotal} \quad (4)$$

The total amount of lignin recovered, $R_{Lig,}$ can then be calculated (Eqs. (5) and (6)) where $m_{Lig,pp}$ is the total mass of lignin precipitated after 4 passes in the SDE:

$$m_{Lig,pp} = m_{Lig,BLTotal} - m_{Lig,PBLTotal} \quad (5)$$

$$R_{Lig} = \frac{m_{Lig,pp}}{m_{Lig,BLTotal}} \times 100 \quad (6)$$

#### 3.3.2. Condensate recovery

The volume of the condensate collected in the round bottomed flask

after each pass on the SDE had occurred was measured using a volumetric cylinder.

### 3.4. Product purity

#### 3.4.1. Fourier transform infrared (FTIR) spectroscopy

An Agilent – FTIR Cary 630 was used for the Attenuated Total Reflection - Fourier Transform Infrared Spectroscopy (ATR-FTIR) analysis of the dried precipitate, in order to identify key species in the product composition and potential impurities. Infrared spectra were collected in the wavenumber range, 650 – 4000 $cm^{-1}$, with all samples being scanned 64 times at a resolution of 4 $cm^{-1}$.

#### 3.4.2. High performance liquid chromatography (HPLC)

Sugar, ethanol, acetic acid, formic acid and levulinic acid, 5-HMF and furfural present in the black liquor, condensate and lignin precipitate samples were quantitatively determined using HPLC.

To determine ethanol, acetic acid, formic acid and levulinic acid concentrations in the black liquor and condensate, a Shodex SH1011 column was used at 55 ℃. 0.6 ml $min^{-1}$ of 0.005 M $H_2SO_4$ in HPLC water was used as mobile phase. The sugar, 5-HMF and furfural concentrations were determined with a Shodex SP0810 column at 80 ℃. 1 ml $min^{-1}$ of HPLC water was used as the mobile phase.

When determining the concentration of ethanol in the condensate, the condensate was diluted by a factor of 10 using HPLC water to ensure the ethanol concentration was in the measurement range of the RI detector. When analysing BL samples, the lignin first had to be removed to prevent fouling inside the HPLC column, otherwise precipitation would occur once the BL sample was injected into the aqueous mobile phase. The BL was removed using the method outlined in Section 3.3.1. and the resulting supernatant was then analysed.

Sugar and organic acid contaminants in precipitated lignin samples were leached out by washing approximately 0.1 g of lignin precipitate with deionised water. The samples were left to leach overnight before being vortexed for 1 min. The sample was then centrifuged at 3500 $\times g$ for 10 min and the supernatant analysed for the presence of sugars and acetic, formic and levulinic acid contaminants using the Shodex SH1011 column with the same method outlined above. To ensure that contaminates were not locked up in the precipitate, separate analysis was carried out where approximately, 0.1 g of lignin was redissolved in 5 ml of ethanol. The lignin was then reprecipitated with pH 2.1 acidified water and the sample was centrifuged and supernatant analysed as before.

All samples were filtered with 0.45 μm PTFE hydrophilic syringe filters to remove any solids present prior to injection into the columns.

#### 3.4.3. Differential scanning calorimetry

Differential Scanning Calorimetry (DSC) analysis was done to determine the glass transition temperature ($T_g$) of the precipitated lignin. A small sample (1–15 mg) was contained within an aluminium 20 μL sealed TA tzero pan and placed in a DSC cell. A second sealed TA tzero pan without sample was used as reference. To remove any moisture contained in the sample and erase the thermal history of the sample, the temperature was first ramped to 200 °C at 20 °C $min^{-1}$, held isothermally for 5 min, and then ramped down to 30 °C at 20 °C $min^{-1}$ and kept isothermal for 5 min longer. The sample was then carried out by heating to 200 °C at 20 °C $min^{-1}$. The $T_g$ was then found using the second heating curve on the TA universal analysis 2000 software. The $T_g$ of the lignin samples was compared to reference the BioPiva 395 Kraft lignin provided by UPM and Organosolv lignin produced by FhG using the falling film evaporation method as described in [5].

### 3.5. Particle size

A LEICA DM500 microscope and an ICC50 digital microscope camera were used to image the lignin precipitate samples. The microscope was calibrated using a stage micrometre and the LAS EZ software. A few drops of a sample obtained from the SDE were imaged each time. Particle size distributions were determined by image analysis using the analyse particles setting in Fiji ImageJ 2.1.0/1.53c software.

### 3.6. Energy consumption

The energy consumption of the SDE, pumps, heaters, chillers and other equipment was measured using RS PRO Energy Meters. Readings were taken before and after each pass of the black liquor through the SDE. These data combined with the process streams were used for the energy consumption calculations for the SDE.

### 3.7. Statistical analysis

Statistical analysis was carried out on Origin Pro 2019 and Minitab. ANOVA analysis was employed to determine the statistical significance of the operating conditions on product and condensate recovery and particle size.

## 4. Results and discussion

### 4.1. Lignin recovery

Conceptually, the processes occurring over the disc can be envisaged as two sequential processes taking place across distinct disc sections. Starting from the feed point near the centre of the disc, there is a heating section wherein the feed undergoes sensible heating up to its boiling point, whilst the liquid travels from the centre outwards. Once boiling point is reached, the feed enters the evaporation section of the disc where vigorous evaporation takes place through boiling over the disc surface. As lignin is only soluble in the ethanol, and ethanol is more volatile than water, evaporating the ethanol from the BL makes the BL richer in water, and generates greater levels of supersaturation, which cause the lignin to precipitate.

Fig. 3 shows how increasing the number of passes through the SDE increases the lignin recovery. This is because more ethanol evaporation occurs after each pass, leaving the BL depleted in ethanol and richer water, which drives lignin supersaturation. For the majority of the experiments, and therefore for the subsequent data presented, only lignin recovery after 3 and 4 passes through the SDE were studied, as the amount of precipitate recovered during earlier passes was small.

The impacts of hydrodynamic operating conditions such as disc speed, BL flow rate, and disc surface texture on the lignin recovery after

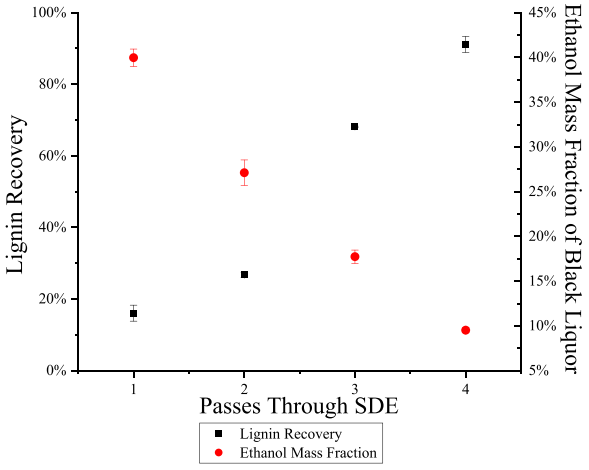


**Fig. 3.** Lignin recovery (measured in relation to the initial amount of lignin in unprocessed BL) and ethanol composition of the BL as a function of the number of passes in the SDE. This experiment was carried out at a feed flowrate of 1 ml $s^{-1}$, 2400 rpm speed, over a smooth disc surface, heated to 100 ℃.

4-disc passes are shown in Fig. 4. The greatest lignin recovery of 94.6 % was found on a smooth disc at 1200 rpm and 1 ml $s^{-1}$ flow rate. The flow rate is shown to have the greatest impact on the lignin recovery ($p$ = 0.000), with lower flow rates leading to higher lignin recoveries at all disc speeds (the average lignin recovery at 1 ml $s^{-1}$ was 92.0% *vs.* 50.7 % at 5 ml $s^{-1}$). The disc speed has a less significant impact on lignin recovery ($p$ = 0.312), with lower disc speeds marginally increasing the lignin recovery (average for all experiments at indicated disc speeds, 74.7% at 1200 rpm *vs.* 69.8 % at 2400 rpm). The smooth disc surface was also found to outperform the grooved surface by a small margin (average of 75.6% *vs* 68.8 % for smooth and grooved surfaces respectively regardless of other operating conditions), making the disc surface texture an influential factor ($p$ = 0.019).

One important consequence of lowering the flowrate is a smaller amount of fluid needing to be heated up and vaporised in the SDE so that there is a higher amount of heat energy transfer per unit mass of fluid on the disc. This would allow more solvent to be evaporated with a rapid onset of high supersaturation levels and precipitation. The impact of the flowrate on both the residence time and film heat transfer coefficient is equally relevant in this context. At lower flowrate, an increase in residence time, $t_{res}$, is expected based on Eq. (7) [31]:

$$t_{res} = \left(\frac{81\pi^2\nu}{16\omega^2Q^2}\right)^{\frac{1}{3}}\left(r_o^{\frac{4}{3}} - r_i^{\frac{4}{3}}\right) \quad (7)$$

where $\nu$ is the kinematic viscosity, $\omega$ is the disc rotation speed, $Q$ is the flow rate, and $r_o$ and $r_i$ are the outer and inner radius respectively. This provides more time for evaporation to occur, enabling greater levels of lignin supersaturation to be achieved. This hypothesis is supported by the findings in Fig. 5, where a clear positive relation between residence time and lignin recovery can generally be seen at all flowrates except at the highest value of 5 ml $s^{-1}$. Under these conditions, the process is residence time controlled, whereas at the highest flowrate it is heat transfer controlled. Further elaboration about these trends is highlighted next in the discussion section on the influence of disc speed. Fig. 5 also shows that for 4 passes the total residence time of the BL in the SDE is <1 s, which is a significant process intensification step, as distillation and evaporation are typically time consuming processes, especially in conventional equipment.

Reducing the flowrate also decreases the film thickness of the BL on the disc, $\delta$, as a function of the radius, $r$, as shown in Eq. (8) [24]:

$$\delta = \left(\frac{3\nu Q}{2\pi\omega^2 r^2}\right)^{\frac{1}{3}} \quad (8)$$

A thinner film reduces the thermal diffusion pathway for heat transfer between the disc surface and the top of the liquid film where evaporation occurs. This significantly affects the heat transfer

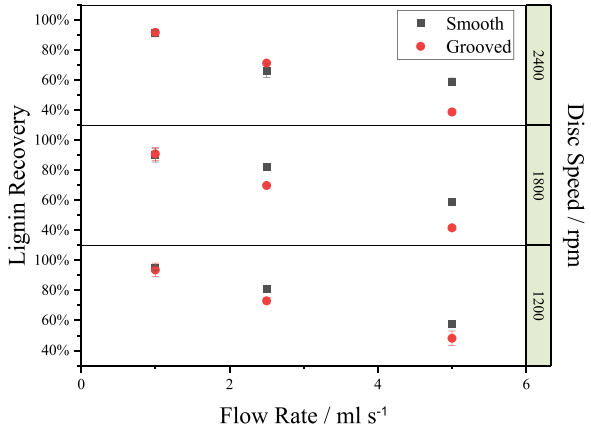


**Fig. 4.** Impact of flow rate, disc speed and disc surface on lignin recovery at disc temperature of 100 °C, after 4 passes through the SDE.

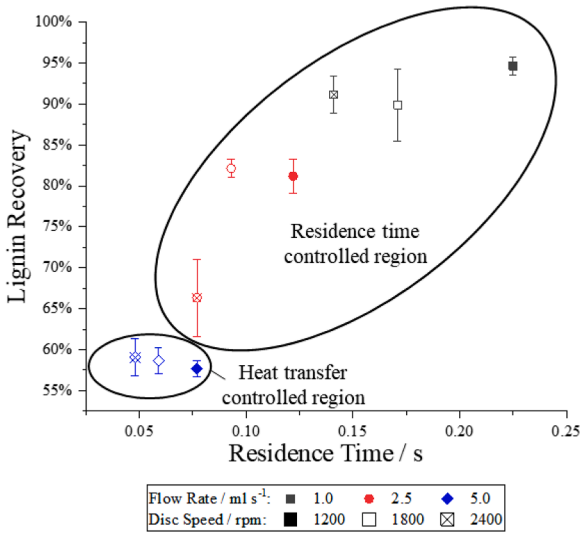


**Fig. 5.** Impact of flow rate, disc speed and residence time on lignin recovery at disc temperature of 100 °C when using a smooth disc, after 4 passes through the SDE, with heat transfer and residence time-controlled regions highlighted.

coefficients in the film, $h$, which is inversely proportional to the film thickness as shown in Eq. (9) [24]:

$$h = \frac{5}{3}\frac{k}{\delta} \quad (9)$$

Where $k$ is the thermal conductivity of the black liquor at its boiling point, modelled as a mixture of 43.5 %(w/w) ethanol and 57.5 %(w/w) water and estimated to be 0.23 W $m^{-1}$ $K^{-1}$ using Aspen Plus. Thus, reducing the flow rate plays a large role in increasing the heat transfer coefficient, and therefore the heat transfer rate, enabling more lignin to be recovered, as observed in Fig. 6.

As observed in Fig. 4, although disc speed had less of an impact on the lignin recovery than flowrate, there are interesting trends to note. While higher disc speed is expected to reduce the film thickness (Eq. (8)) and elevate the film heat transfer coefficient (Eq. (9)), similarly to the effect of lower flowrate, this SDE operational parameter has to be optimised to also achieve sufficient residence time in any given process. Most interestingly, it is also evident from Figs. 5 and 6 that the highest

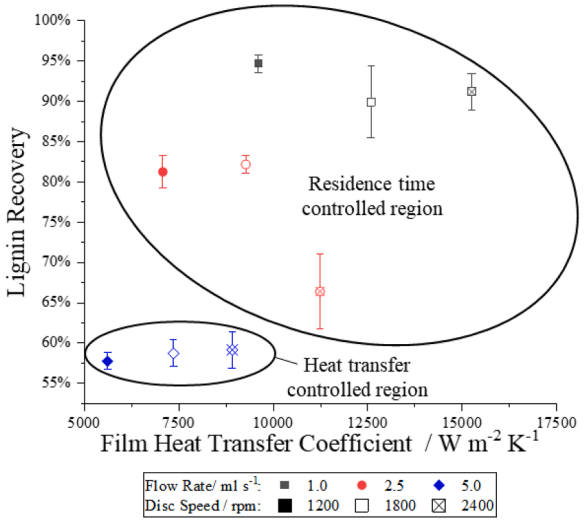


**Fig. 6.** Impact of flow rate, disc speed and film heat transfer coefficient based on average film thickness across the disc on lignin recovery, at a disc temperature of 100 °C and after 4 passes through the SDE over a smooth disc surface, with heat transfer and residence time-controlled regions highlighted.

disc speeds of 2400 rpm are more beneficial when combined with the highest flowrates of 5 ml $s^{-1}$, whereby the film thickness can be effectively suppressed to achieve higher heat transfer coefficients. Under such conditions of high flowrate, the process appears to become more heat transfer limited, presumably because of lower energy input per unit mass, which explains the observed beneficial impact of operating at higher disc speeds to counter these limitations. In contrast, at lower flowrates, the operating regime shifts to residence time control under conditions of high rates of energy input per unit mass where the lignin yields are dictated by residence time rather than heat transfer. Thus, the highest yields are attained at the lowest disc speed of 1200 rpm with these lower flowrates, where residence time is maximised while the film heat transfer coefficients were still more than sufficient to achieve the maximum evaporation rate, as seen in Figs. 5 and 6. It is therefore postulated that the change in regime in this process occurs at a film thickness threshold of ~40 μm whereby films below this threshold are able to readily overcome heat transfer limitations in the evaporation step (Figure S1). These results highlight the complex interactions between flowrate and disc speed, which must be elucidated to identify the interplay of multiple phenomena affecting the SDE evaporation process.

The smooth disc was found to be marginally more effective than the grooved disc at recovering lignin, with the mean lignin recovery increased by 6.8 % on the smooth disc. This is contrary to predictions based on previous literature that reports grooves enhancing the film heat transfer coefficient [23]. However, that study was conducted on a much larger disc (360 mm diameter in reference [23] *vs.* 100 mm in this study) and at lower disc speeds (250 - 890 rpm *vs.* 1200–2400 rpm in this study). In the present study, there may have been an insufficient number of grooves on the disc to generate significant surface effects resulting in a negative impact on lignin recovery. Furthermore, some black liquor may have been thrown off the disc after exiting the groove, especially at high flow rates and disc speeds, reducing the wettability of the disc surface and contributing to film breakdown, decreasing the efficiency of the process.

The impact of using a grooved disc surface and varying the disc speed can become more pronounced on a larger disc system in which the fluid is passed a single time through the disc, as the differences in residence time and film thickness become more noticeable in the large-scale system. This shown in both Eq. (7) and (8) where larger radii increase residence time and reduce film thickness towards the edge of the disc. The additional surface area also allows for an increased number of grooves on the disc, enabling them to have a greater impact on the system. Care must be taken to ensure that the film thickness is not reduced excessively by increasing the disc radius, as a film thickness of less than ~20 μm can result in film breakdown causing rivulet flow and reducing the effective surface area of the disc [22]. A larger disc will also experience an increase the shear rate (Eq. (10), [32]) which may flatten wave formation at extreme rates of shear [23]:

$$\gamma_{max} = \frac{\omega^2 r}{\nu} = \left(\frac{3Q\omega^4 r}{2\pi\nu^2}\right)^{\frac{1}{3}} \quad (10)$$

Where $\gamma_{max}$ is the maximum shear rate at any radial position $r$ from the centre of the disc.

The surface plots generated from a model of the experimental data for the smooth disc (Fig. 7a and Eq. (11)) had an $R^2$ of 0.9255 while for the grooved disc (Fig. 7b and Eq. (12)) had an $R^2$ of 0.9360, indicating a good fit between the data and the models in both cases. The models also demonstrate how varying flow rate has a much greater impact on lignin recovery than disc speed or disc surface. The interactions between disc speed and flow rate were found to be insignificant and therefore were not included in the model.

For the following models of predicted lignin recovery, $Q$ is the flowrate in ml $s^{-1}$ and $N$ is disc speed in rpm.

Smooth disc model:

$$Lignin\ recovery\ = 107.46 - (0.00471 \times N) - (8.241 \times Q) \quad (11)$$

Grooved disc model:

$$Lignin\ recovery = 105.25 - (0.00414 \times N) - (10.233 \times Q) \quad (12)$$

The models are applicable in the following ranges:

$$1200\ rpm \leq N \leq 2400\ rpm$$
$$1\ ml\,s^{-1} \leq Q \leq 5\ ml\,s^{-1}$$

From the models (Fig. 7, Eq. (11) & (12)), the optimum point for lignin recovery was 1200 rpm and 1 ml $s^{-1}$ for both disc surfaces, whereby the impact of the operating conditions on film thickness, wave formation, residence time and heat transfer result in maximised lignin precipitation as discussed above. The negative coefficients for both disc speed and flow rate reflect the inverse relationship between these parameters and lignin recovery, while the large coefficient for flow rate highlights its importance on lignin recovery. These trends were in line with experimental observations which is underlined by the experimental data for both disc types deviating from the model by no more than 5.5 % on average. The parity plot shown in Figure S2 in the Supplementary Information provides further evidence for the agreement between experimental and model data.

Lower flow rates could not be used in this set up without pulsed flow occurring due to the peristaltic pump limitation. Lower flow rates would

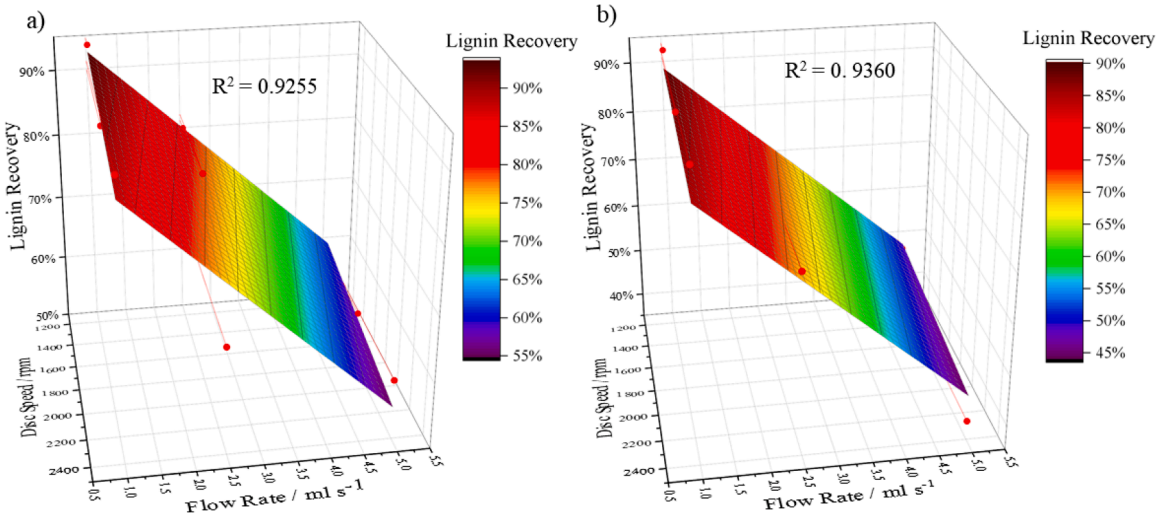


**Fig. 7.** Response surface plots obtained for lignin recovery on the smooth (a) and grooved (b) discs.

also risk breakdown of the thin film into rivulet flow resulting in the heat and mass transfer enhancements being lost [33]. Lower disc speeds were deemed unsuitable in this study to achieve optimal characteristics of the film flow and transfer processes on the disc, where film thicknesses would have been above the threshold value identified in this study (Figure S1).

Negligible amounts of fouling occurred in the evaporator due to sticky lignin forming at high temperatures and encrusting on the walls and disc of the SDE. Reducing the temperature required for evaporation by applying a vacuum could further minimise fouling as lignin becomes less sticky at lower temperatures [5] with additional scope for reducing the required heating duty. SDEs operating under vacuum conditions have successfully been demonstrated in an earlier study [30].

### 4.2. Condensate recovery

As expected, there is a strong correlation between lignin and condensate recovery, which is shown in Fig. 8, as ethanol removal leads to an increase in lignin supersaturation, resulting in precipitation. HPLC data has confirmed that ethanol concentration decreased in the black liquor with each pass through the SDE, with lower ethanol concentrations returning greater lignin yields due to increased supersaturation (Fig. 3).

Fig. 8 is very clear on the fact that the main factor influencing condensate recovery is flow rate ($p = 0.000$ for flow rate *vs.* $p = 0.349$ for disc speed and $p = 0.042$ for disc surface), supporting the results of the lignin recovery discussed in Section 4.1. A lower flow rate resulted in a greater condensate recovery which increased lignin supersaturation and therefore the amount of lignin precipitation.

When analysing the condensate recovered using HPLC, it was found that the concentration of ethanol to be between 25 - 45 %(w/w). Trace amounts of formic acid, acetic acid, levulinic acid, 5-HMF and furfural were also found (< 1 %(w/w) in total), nevertheless, it is estimated the vast majority of the condensate is made of just ethanol and water.

### 4.3. Lignin product purity

#### 4.3.1. HPLC analysis

When analysing the washings of the lignin precipitate after SDE precipitation and the supernatant obtained after the SDE precipitated lignin was redissolved and reprecipitated with acidified water, no sugars or organic acids were detected. The sugars and organic acids are the compounds (besides lignin) present in higher concentrations in the BL and therefore the most likely sources of contamination in the precipitate which is why these compounds had a particular emphasis on their detection. Additionally, other expected impurities would be extractives of volatile nature that could be evaporated jointly with the ethanol or inorganic ions which are most likely to be water soluble and therefore easy to wash from the precipitate surface if they do precipitate. This means the lignin precipitated from the SDE was of a very pure nature and that the other main species in solution in the BL are not being trapped inside the precipitate particles.

#### 4.3.2. FTIR

Fig. 9 displays the spectra of the dried lignin precipitation samples obtained from the evaporative precipitation experiments with the greatest yields. Although the region analysed spans the 650 – 4000 $cm^{-1}$ wavenumber range, the fingerprint region (650 – 1800 $cm^{-1}$) is of most interest as it contains the most spectral information about the molecular composition of the precipitate. The FTIR spectra obtained were compared to literature data and reference spectra [34,35,36,37,38] and the peaks were assigned to the various lignin functional groups. The FTIR is a qualitative technique, detecting if the functional groups present are associated with lignin or impurities and does not quantify the species present. No differences in the FTIR spectra were found when different operating conditions were used.

The band between 1650 – 1750 $cm^{-1}$ represents C = O stretching of unconjugated ketones, carbonyls and ester groups (mostly in the hemicelluloses). The peak at 1594 $cm^{-1}$ is associated to benzene rings while, aromatic skeletal vibrations of guaiacyl and syringyl units are the peak at 1508 $cm^{-1}$. Deformation in -$CH_2$, -$CH_3$ groups is the peak at 1458 $cm^{-1}$ and deformation in -CH is for 1421 $cm^{-1}$. 1321 $cm^{-1}$ accounts for C—O bonds in syringyl rings and 1275 $cm^{-1}$ accounts for guaiacyl rings. 1211 $cm^{-1}$ is C—O bonds in ether groups. 1140 $cm^{-1}$ is assigned to C—H bonds in guaiacyl rings. 1110 $cm^{-1}$ is C—O deformation of secondary alcohols and C—H in plane deformation in guaiacyl and syringyl rings. 1028 $cm^{-1}$ represents C – H deformation in hemicellulose and C – O stretch in polysaccharides. A larger peak at 1028 $cm^{-1}$ than the reference sample would indicate possible sugar contamination making is a good test for lignin purity. The final peaks at 910 $cm^{-1}$ and 829 $cm^{-1}$ are associated with C—H deformation and aromatic rings respectively.

The spectra for Organosolv lignin obtained using a falling film evaporator at FhG, using the process described in Schulze [5] is included as a reference point. The lignin precipitated and the reference sample have almost identical FTIR fingerprints, further highlighting the fact

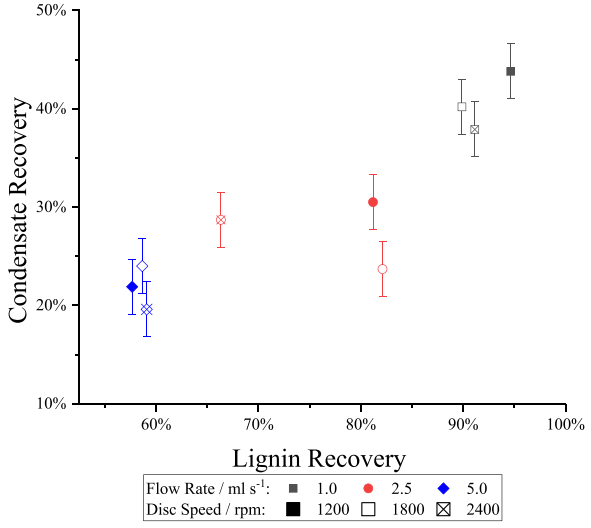


**Fig. 8.** Lignin recovery as percentage of total mass of precipitable lignin *vs* Condensate recovery as percentage of the raw BL mass processed on a smooth disc.

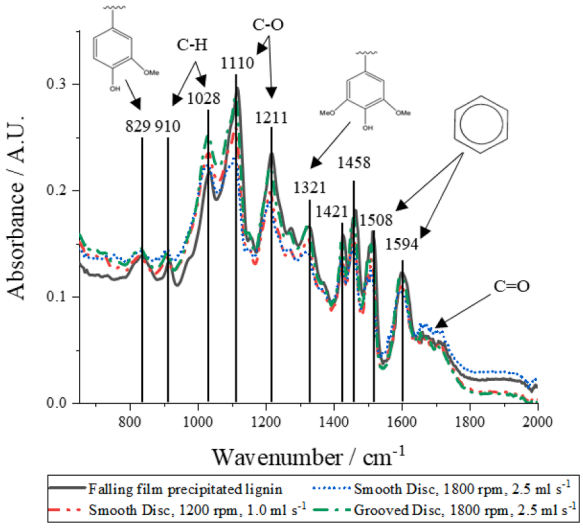


**Fig. 9.** Fingerprint FTIR spectra of the precipitated lignin, with some of the key functional groups highlighted.

that the SDE yields high purity lignin with minimal contaminants.

#### 4.3.3. DSC

According to the DSC findings, the lignin displays a degree of thermoplastic behaviour, with glass transition temperatures between 110 – 167 °C (Fig. 10). A sample of the lignin obtained by precipitation in the falling film evaporator at FhG [5] was also analysed for reference, and a glass transition temperature of 117 °C. These values are all well within the temperature range of 90 – 180 °C reported in the literature for lignins which have undergone thermal treatment [39,40], confirming the suitability for further thermal processing into other end products.

By itself the absence of sugars or organic acids in the HPLC cannot indicate that the precipitated lignin is of a high purity as this technique only quantifies identifiable peaks. However, the HPLC results did not reveal additional unidentified peaks. The FTIR spectra also lacked unexpected and unexplainable peaks, and peaks for identifiable impurities were also not identified. All peaks were close matches that of the reference lignin samples. Additionally, the DSC analysis identified glass transition temperatures within the expected ranges in comparison with the reference lignin samples. Therefore, the combination of techniques suggests the purity of lignin obtained is indeed very high, and that no impurities above the detection limits are trapped within the particles or are retained adsorbed to the particles surface after precipitate washing.

### 4.4. Particle size

Samples of the lignin precipitate in suspension in the BL were analysed by optical microscopy. As shown in Fig. 11(a) and (b), particles averaging between 3 – 9 μm in diameter, with minor agglomeration, were formed after 4 passes through SDE.

Particle size information was extracted from the optical microscopy images through image analysis methods, as detailed in the methodology section. As shown in Fig. 12, particles produced on the grooved disc are on average slightly larger than with a smooth disc. This is thought to be due to additional particle collisions arising from induced turbulence in the grooves of the disc leading to a higher degree of agglomeration. This is supported by previous research [27] which found that the impact of disc surface on particle size is generally less profound than on the increase in range of particle size distribution.

The flow rate and disc speed had no statistically significant impact ($p > 0.05$) on the lignin particle size in the ranges studied for these parameters. This signifies that the trend where particle size decreases at 1200 and 2400 rpm at higher flow rates and the reverse trend where particle size increases with flow rate at 1800 rpm is insignificant. The narrow average size of particles obtained also highlights that uniform processing conditions prevailed in the SDE and that size differences are mainly due to experimental variation. This can be attributed to effective mixing on the disc at all operating conditions ensuring uniform supersaturation across the film layer and leading to a high nucleation rate, with minimal particle growth. It is likely the low residence time (<1 s) led to minimal particle growth, which is usually a slow process. The high shear forces may also have broken apart many of the aggregates which form on the disc. Fig. 13 shows a typical particle size distribution for the lignin precipitate measured using microscopy. The vast majority of the particles are around the 1–10 μm range although a few larger particles, thought to be agglomerates, have also been observed.

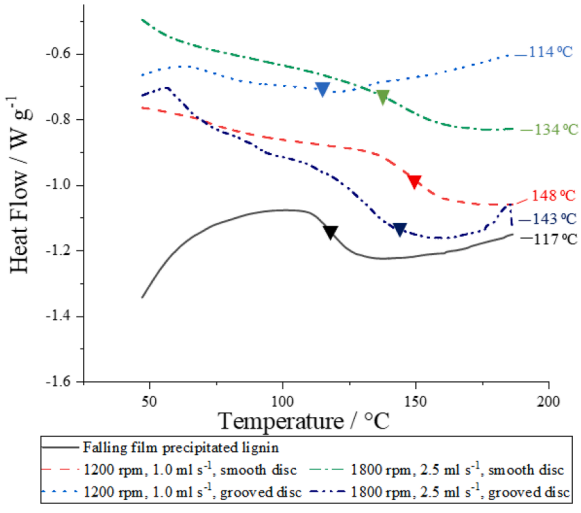


**Fig. 10.** DSC thermogram for lignin precipitate. The glass transitions for each sample indicated are indicated by triangles.

The optical microscopy technique for particle size measurement has been validated using dynamic light scattering, with comparison data shown in Figure S3 in the Supplementary Information. The lignin particle size characteristics are comparable with the particle sizes produced in the falling film evaporator, whereby Schulze [5] found that primary lignin particles of 1 – 2 μm were formed. However, in the falling film evaporator there was also significant agglomeration above 20 μm, unlike in the SDE. The low residence time and high shear rates in the SDE is thought to be why agglomeration is less prevalent compared to the falling film, despite a higher temperature being used. The falling film on the other hand has a much higher residence time than the SDE (4 h *vs.* < 1 s) which enables more time for particle growth and agglomeration to occur. That precipitation occurred in such a short time period in the SDE signifies that the induction time for particles forming is very short, indicating a high degree of supersaturation is reached. Therefore, high nucleation rates and low rates of particle growth are expected [41] which is reflected in the data presented. The regular size and voidage between particles produced in the SDE made filtering and washing of the lignin precipitate easy to carry out with preliminary filtration tests showing promising results, achieving a flux of 773 L $m^{-2}$ $h^{-1}$ when using 1.2 μm pore size filter paper.

### 4.5. Comparison to state-of-the-art industrial process

Schematics demonstrating estimated energy inputs into the lignin precipitation processes in the falling film evaporator and SDE are displayed in Figs. 14 and 15 respectively. The energy consumption for the SDE were obtained experimentally using energy meters on all of the processing equipment in combination with the process streams, while the information about the CSTR and FFE, including energy consumption and flow rates, were kindly provided by FhG.

The falling film evaporator set up is described in reference [5]. Black liquor was mixed with ultrapure water in the stirred tank to form 220 kg of dispersion with 6 %(w/w) ethanol. The dispersion was then pumped through the falling film evaporator at 694 ml $s^{-1}$. The falling film evaporator was composed of vertical tubes, with a total heat transfer area of 3.5 $m^2$. Gravity pulled the fluid down the pipes creating a film on the tube walls. 52 °C steam was used to provide the thermal energy for evaporation as the process was operated at 145 mbar, reducing the boiling point of the black liquor. Black liquor and make up water were constantly added to the CSTR in order to keep the ethanol concentration between 6 and 9%(w/w) ethanol, to make up for the ethanol and water losses during evaporation. The level of the tank was not constant: the feed flows were continuous, but once the CSTR exceed 400 kg, some of the precipitate suspension was discharged (typically 100 kg $h^{-1}$) to the lignin dispersion vessel.

The SDE process was as previously discussed in the experimental section, and the heat flows in the process used for the benchmarking study are shown in Fig. 15. There was a large difference in scale between the SDE and falling film evaporator. The BL was also diluted with water to 6%(w/w) ethanol prior to evaporation in the falling film evaporator, compared to 43%(w/w) ethanol in the unprocessed BL used in the SDE. Therefore, whenever possible, the benchmarking values in Table 3 were normalised to reduce their dependency on product scale and allow

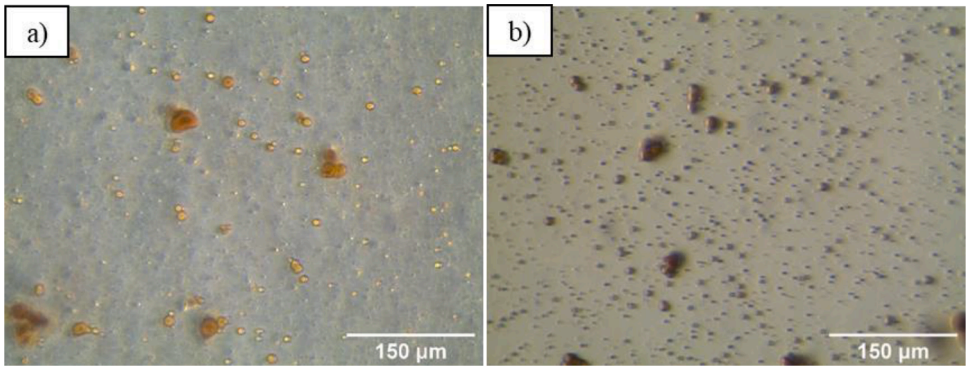


**Fig. 11.** (a) Lignin precipitate after 4 passes through the SDE at 1 ml $s^{-1}$, 1200 rpm, smooth disc at ×400 magnification, and (b) Lignin precipitate after 4 passes through the SDE at 1 ml $s^{-1}$, 1200 rpm, grooved disc at ×400 magnification.

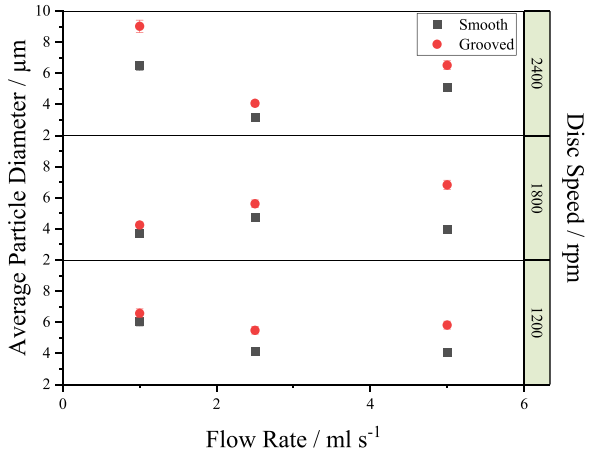


**Fig. 12.** Impact of SDE operational parameters on average particle size.

easier comparisons to be made between the two processes. A more detailed breakdown of the energy consumption calculations can be found in Section S4 of the Supplementary Information.

As Table 3 highlights, the SDE has successfully intensified the evaporative precipitation of lignin. Whilst both processes have virtually the same lignin recovery, the intensified process has minimised the BL processing time by over 14,000×, resulting in less risk for thermal degradation of the sugars in solution, and smaller equipment size with 11.8× higher lignin recovery rate per unit of volume of black liquor processed. The energy consumption per mass of lignin produced is reduced by 23 % which should also translate to a similar reduction in $CO_2$ produced during the process.

The intensification in the SDE is due to a higher overall heat transfer coefficient and large surface area per unit volume of fluid, both of which drive the evaporation process resulting in a much shorter residence time to achieve similar lignin recoveries. This allows the feed to be processed quickly, minimising thermal losses and ensuring a consistent product. The overall heat transfer coefficient, $U$, was determined experimentally using Eq. (13):

$$U = \frac{q}{A \times \Delta T_{lm}} \tag{13}$$

Where $q$ is the heat transfer rate, $A$ is the heat transfer area, and $\Delta T_{lm}$ is the logarithmic mean temperature different between the hot and cold fluids.

It is to be noted that the overall heat transfer coefficient values obtained are a conservative estimate, as it is likely that the rate of heat input, calculated based on the amount of vapour formed and its latent heat, was underestimated due to a constant latent heat value employed corresponding to that of the initial black liquor mixture. In reality, the latent heat will increase during the process as the mixture becomes more concentrated in water and depleted in ethanol, as the water has a higher latent heat than ethanol.

The experimental estimates for the overall heat transfer coefficient values as a function of the radius, $U(r)$, were checked using theoretical correlations for the heat transfer coefficient (Eqs. (14) [24] - (16) [43]):

$$h_{BL}(r) = \frac{5}{3} \times \frac{k_{BL}}{\delta} \tag{14}$$

$$\frac{h_{Therminol}(r) \times d_e}{k_{Therminol}} = j_h \times Re \times Pr^{0.33} \tag{15}$$

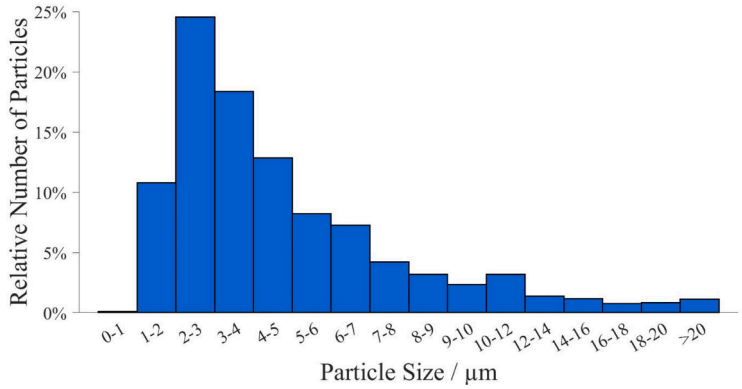


**Fig. 13.** Particle size distribution of lignin particles determined using optical microscopy after 4 passes through the SDE at 2.5 ml $s^{-1}$ and 1800 rpm, over a smooth disc.

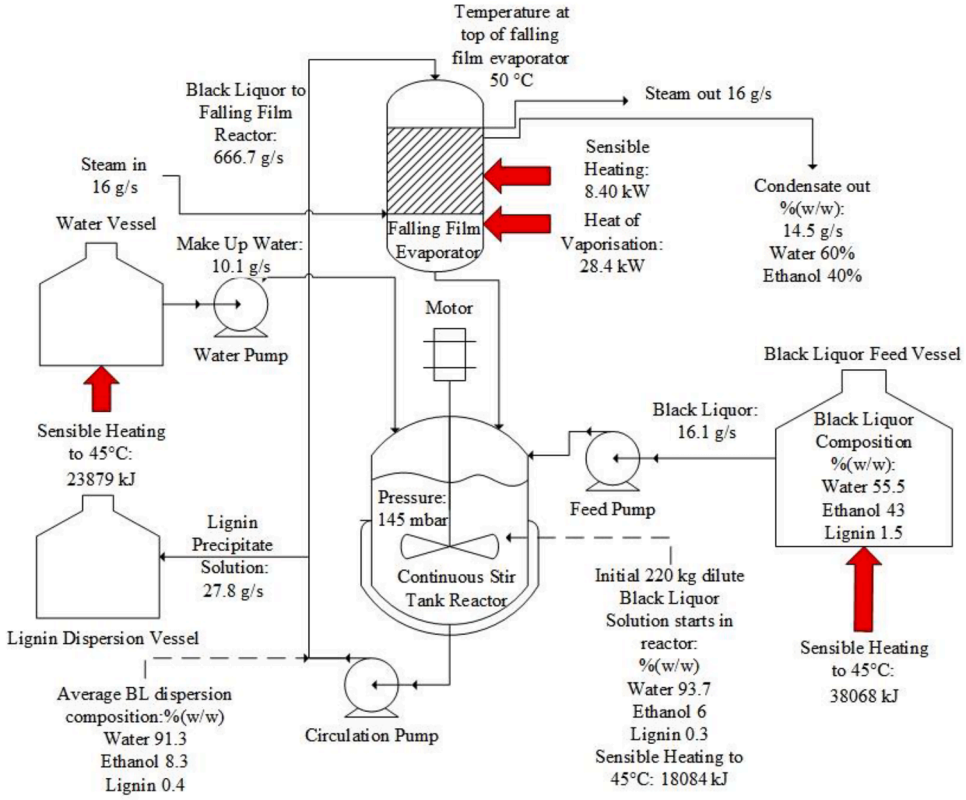


**Fig. 14.** Schematic of precipitation of lignin using a falling film evaporator including known energy consumption, compositions, and flow rates.

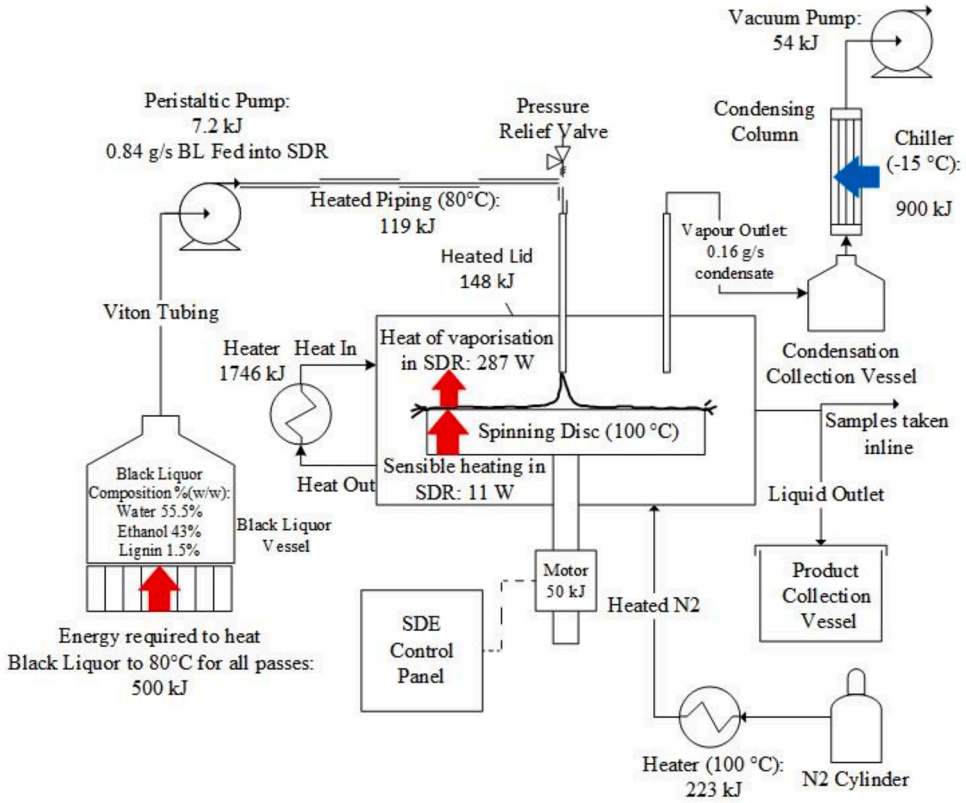


**Fig. 15.** Schematic of precipitation of lignin using an SDE including known energy consumption, compositions, and flow rates.

**Table 3**
Comparison of lignin precipitation process in the CSTR and falling film evaporator *vs.* the SDE. Values per mass unit of lignin produced unless specified.

| Process | CSTR and Falling Film Evaporator (pilot scale) | SDE (lab scale) 1 ml $s^{-1}$, 1200 rpm |
|---|---|---|
| Lignin Recovery | 96 % | 95 % |
| Residence Time | 4 h | ~ 1 s |
| Lignin recovery rate (per volume of BL) / g $L^{-1}$ $h^{-1}$ | 3.23 | 38.1 |
| Energy consumption[†] / kJ $g^{-1}$ | 299 | 229 |
| Energy cost[†] [42]/ £ $kg^{-1}$ | 16.79 | 12.84 |
| Overall heat transfer coefficient / kW $m^{-2}$ $K^{-1}$ | 1.92 | 2.04 ± 0.11 |
| Particle size / μm | 1 – 2 μm Significant agglomeration occurred | 3–9 μm Minor agglomeration occurred |
| Footprint[‡] | 550 L of BL processed + 500 L of water. The CSTR and falling film evaporator set up is approximately 0.8 m × 2 m × 3.7 m. | 550 L of BL processed and no diluting water. SDE rig with 87.4 cm diameter disc approximately 1 m × 1 m × 1 m after accounting for reactor jacket and motor. |

[†] Determined considering 8 h processing time to level energy start-up costs.
[‡] Footprint of SDE with capacity to process 550 L of black liquor in the same time scale as the falling film process.

$$U(r) = \frac{1}{\frac{1}{h_{BL}(r)} + \frac{x}{k_{stainless\ \ steel}} + \frac{1}{h_{Therminol}(r)}} \quad (16)$$

where $h_{BL}(r)$ is the film heat transfer coefficient for the BL as a function of the disc radius, $h_{Therminol}$ $(r)$ is the film heat transfer coefficient for Therminol under the disc as a function of the radius, $d_e$ is the hydraulic diameter for Therminol flow under the disc, $j_h$ is the Chilton-Colburn $j$ factor for heat transfer, $Re$ is the Reynolds number for Therminol flow under the disc, and $Pr$ is the Prandtl number for Therminol.

The overall heat-transfer coefficient was calculated as a function of the radial distance $r$ from the centre of the disc centre (Eq. (16)), and the average value of 2.8 kW $m^{-2}$ $K^{-1}$ was in good agreement with the experimental values (2.04 kW $m^{-2}$ $K^{-1}$).

One major advantage of the SDE process is that the black liquor in the SDE stream is not diluted with water addition in contrast to the CSTR-FFE process, making the SDE process more resource and energy efficient as less liquid needs to be boiled off. The concentrated BL from the SDE will also be easier to process downstream as the narrow particle size distribution of the lignin is ideal for filtration and the concentrated BL stream will enable easier recovery of the hemicellulose.

The footprint of the SDE is 5.9× less than the falling film system, for an SDE scaled up to the same capacity of the FFE system. This reduction is because the lower flow rates required to process the same amount of black liquor combined with the lack of black liquor predilution, results in a lower reactor volume. Scaling up the SDE according to an established methodology [22] resulted in a disc of 88 cm diameter disc operating at 19 ml $s^{-1}$ and 600 rpm for precipitation to occur in a single pass. The capital costs of the SDE system is expected to be lower than the falling film evaporator due to its small size, reduced interconnecting pipework and no predilution requirements for the black liquor.

When evaporative precipitation of lignin was investigated by Schulze [5,44] using a lab scale continuously operated FFE, fouling was found to be a major problem with up to 41 % of the lignin lost to fouling at conditions similar to the pilot plant scale. However, recoveries of up to 99 % were achieved when the temperature of the falling film evaporator was kept below 50 °C. While this recovery is excellent, the mean residence time of the liquor in the system was 650 min and only 1.3 kg of BL dispersion was processed. This emphasizes how the SDE intensifies the evaporative process as it handles over 11× the mass in the same time scale with no dilution.

The SDE demonstrates successful process intensification compared to other methods of lignin precipitation. Botello et al. 1999 [11] only recovered <75 % and Liang et al. 2016 [45] recovered <75 % and <90 % of lignin using antisolvents at lab scale. The dilution of the downstream HMC containing solution meant additional distillation steps for solvent recovery were required increasing their capital and energy costs as well as the process footprint and materials used compared to the SDE. Furthermore, as dissolved lignin is often polydisperse, certain anti-solvents may only be effective for a certain lignin fraction leaving some behind in the solution [46] limiting lignin recovery. Antisolvents used with lignin can also act as antisolvents for sugars making them undesirable for use in lignin precipitation [47].

The SDE also outperformed other methods of intensifying evaporation. A wiped film evaporator, composed of a heated cylindrical tube with inner rotating wiper system, where the fluid flow is driven downwards by gravity. was found to achieve an overall heat transfer coefficient of 1.89 kW $m^{-2}$ $K^{-1}$ when evaporating monoethylene glycol [48]. This is lower than the SDE, likely because the flow is driven by gravity resulting in thicker films. Ultrasound has been shown to improve the overall heat transfer coefficient of a Robert-type calandria evaporator by up to 20 %, to 1.25 kW $m^{-2}$ $K^{-1}$, thanks to the effects of acoustic cavitation and streaming [49]. However, this is still less than that obtained in the SDE. Other falling film systems used for evaporation were also investigated for comparison, however these could not achieve heat transfer coefficients in the film above 7000 W $m^{-2}$ $K^{-1}$ even when converging-diverging tubes are used to enhance performance [50,51].

Nano- and ultra- membrane filtration processes were deemed unsuitable for purification of this specific BL hydrolysate due to the difficulty of separating HMC from lignin oligomers [17]. However, if integrated with the SDE in a pre-evaporation step, it could be a cost-effective method of concentrating BL by removing some of the ethanol present before it is subjected to evaporative precipitation and is worth investigating further.

Further enhancements could be made to the SDE by using a vacuum to reduce the boiling point of the black liquor as done in the falling film evaporator system. This technique has already been demonstrated to work in the SDE [30] so is a promising path of future optimisation. This should also minimise fouling in the SDE even further as the lignin would be less sticky if precipitated at lower temperatures. Using a more thermally conductive material such as aluminium for the disc and increasing the internal heat transfer coefficient of the disc heating system could further enhance the heat transfer process. Multiple SDEs operating in parallel would also increase the process throughput. Finally, using a larger disc would remove the requirement for multiple passes, making the process simpler and more efficient as preheating requirements would be reduced.

## 5. Conclusion

The evaporative precipitation of lignin was successfully carried out using the SDE for the first time, achieving yields of up to 95 %. Optimal operating conditions were found at a disc speed of 1200 rpm and 1 ml $s^{-1}$ flow rate, as this is where the residence time of the order of seconds was maximised under conditions of high rates of heat transfer in the very thin film. A smooth disc was also found to improve lignin recovery compared to a grooved texture, although a larger disc may enable the grooves to have a greater impact on lignin recovery. The average particle size was between 3 – 9 μm with little agglomeration regardless of operating conditions. The purity of the lignin produced was also high

(estimated to be >99 %) as no impurities were detected.

This study demonstrated a successful intensification of the precipitation process as 23 % higher energy efficiency could be achieved in the SDE compared to the CSTR/FFE. The SDE also had a much higher lignin recovery rate (38.1 *vs.* 3.23 g $L^{-1}$ $h^{-1}$) obtained under significantly lower residence time (<1 s *vs.* 4 h) than the CSTR/falling film evaporator without sacrificing purity. Its smaller footprint (5.9× less) even when scaled up should be beneficial in designing more modular, mobile plants for biorefinery applications.

Further improvements could be made to the process by operating the system under vacuum. This would lower the boiling point of the solvent, reducing the energy inputs required and minimise fouling even further as the lignin produced would be less sticky. Scaling up the SDE using a larger disc will also remove the need for multiple passes through the same SDE, increasing throughput and reducing the preheating energy requirements. This could pave the way for the successful implementation of the SDE into future biorefinery applications.

## CRediT authorship contribution statement

**Thomas Carr:** Writing – review & editing, Writing – original draft, Methodology, Investigation, Formal analysis, Data curation. **Fernando Russo Abegão:** Writing – review & editing, Writing – original draft, Validation, Supervision, Project administration, Methodology, Funding acquisition, Conceptualization. **Kamelia Boodhoo:** Writing – review & editing, Writing – original draft, Validation, Supervision, Project administration, Methodology, Funding acquisition, Conceptualization.

## Declaration of competing interest

There are no conflicts to declare.

## Data availability

Data will be made available on request.

## Acknowledgements

This project has received funding from the Bio Based Industries Joint Undertaking under the European Union's Horizon 2020 research and innovation programme under grant agreement No 887226. The provision of Organosolv black liquor, lignin reference samples and the energy consumption data for the industrial process by Dr Ireen Gebauer at Fraunhofer CBP, Leuna, Germany, are gratefully acknowledged.

## Supplementary materials

Supplementary material associated with this article can be found, in the online version, at doi:10.1016/j.cep.2024.109734.

## References

[1] M. Pantaleo, M. Dees, B.S. Elbersen, L. Iriarte, U.R. Fritsche, B. Glavonjic, D. Stojadinovic, T. Zhelyezna, D. Carrez, D8. 1 Overview report on the current status of biomass for bioenergy, biofuels and biomaterials in Europe, S2Biom (2016).
[2] S. Beisl, A. Miltner, A. Friedl, Lignin from micro-to nanosize: production methods, Int. J. Mol. Sci. 18 (6) (2017) 1244.
[3] J. Zakzeski, P.C. Bruijnincx, A.L. Jongerius, B.M. Weckhuysen, The catalytic valorization of lignin for the production of renewable chemicals, Chem. Rev. 110 (6) (2010) 3552–3599.
[4] Z. Strassberger, S. Tanase, G. Rothenberg, The Pros and cons of lignin valorisation in an integrated biorefinery, RSC Adv. 4 (48) (2014) 25310–25318.
[5] P. Schulze, M. Leschinsky, A. Seidel-Morgenstern, H. Lorenz, Continuous separation of lignin from organosolv pulping liquors: combined lignin particle formation and solvent recovery, Ind. Eng. Chem. Res. 58 (9) (2019) 3797–3810.
[6] Matsuhiro B Yáñez-SM, C. Nuñez, S.B. Pan, C.A. Hubbell, P. Sannigrahi, A. J. Ragauskas, Physicochemical characterization of ethanol organosolv lignin (EOL) from Eucalyptus globulus: effect of extraction conditions on the molecular structure, Polym. Degrad. Stab. 110 (2014) 84–194.
[7] R.E. Souza, F.J.B. Gomes, E.O. Brito, R.C. Costa Lelis, A review on lignin sources and uses, J. Appl. Biotechn. Bioeng. 7 (3) (2020) 100.
[8] O.Y. Abdelaziz, D.P. Brink, J. Prothmann, K. Ravi, M. Sun, J. García-Hidalgo, M. Sandahl, C.P. Hulteberg, C. Turner, G. Lidén, M.F. Gorwa-Grauslund, Biological valorization of low molecular weight lignin, Biotechnol. Adv. 34 (8) (2016) 1318–1346.
[9] D. Kim, C.G. Yoo, J. Schwarz, S. Dhekney, R. Kozak, C. Laufer, D. Ferrier, S. Mackay, M. Ashcraft, R. Williams, S. Kim, Effect of lignin-blocking agent on enzyme hydrolysis of acid pretreated hemp waste, RSC adv., 11 (36) (2021) 22025–22033.
[10] P. Sannigrahi, A.J. Ragauskas, Characterization of fermentation residues from the production of bio-ethanol from lignocellulosic feedstocks, J. Biobased Mater. Bioenergy 5 (4) (2011) 514–519.
[11] J.I. Botello, M.A. Gilarranz, F. Rodríguez, M. Oliet, Recovery of solvent and by-products from organosolv black liquor, Sep. Sci. Technol. 34 (12) (1999) 2431–2445.
[12] W.J. Huijgen, J.H. Reith, H. den Uil, Pretreatment and fractionation of wheat straw by an acetone-based organosolv process, Ind. Eng. Chem. Res. 49 (20) (2010) 10132–10140.
[13] A.L. Macfarlane, R. Prestidge, M.M. Farid, J.J.J. Chen, Dissolved air flotation: a novel approach to recovery of organosolv lignin, Chem. Eng. J. 148 (1) (2009) 15–19.
[14] A. Holtz, D. Weidener, W. Leitner, H. Klose, P.M. Grande, A. Jupke, Process development for separation of lignin from OrganoCat lignocellulose fractionation using antisolvent precipitation, Sep. Purif. Technol. 236 (2020) 116295.
[15] M.G. Alriols, A. García, R. Llano-Ponte, J. Labidi, Combined organosolv and ultrafiltration lignocellulosic biorefinery process, Chem. Eng. J. 157 (1) (2010) 113–120.
[16] R.W. Thring, E. Chornet, R.P. Overend, Recovery of a solvolytic lignin: effects of spent liquor/acid volume ratio, acid concentration and temperature, Biomass 23 (4) (1990) 289–305.
[17] A. Arkell, J. Olsson, O. Wallberg, Process performance in lignin separation from softwood black liquor by membrane filtration, Chem. Eng. Res. Des. 92 (9) (2014) 1792–1800.
[18] F. Weinwurm, A. Drljoa, T.L. Silvab, A. Friedla, Principles of ethanol organosolv lignin precipitation: process simulation and energy demand, in: Presented 2014, 17th Conference on Process Integration, Modelling and Optimisation for Energy Saving and Pollution Reduction 39, 2014, p. 583. Pts 1-3.
[19] H. Ma, M. Shen, Y. Tong, X. Wang, Radioactive wastewater treatment technologies: a review, Molecules. 28 (4) (2023) 1935.
[20] D. Yang, B. Leng, T. Li, M. Li, Energy saving research on multi-effect evaporation crystallization process of bittern based on MVR and TVR heat pump technology, American J. Chemical Eng. 8 (2020) 54.
[21] M.A. Pinard, K. Aslan, Metal-assisted and microwave-accelerated evaporative crystallization, Cryst. Growth Des. 10 (11) (2010) 4706–4709.
[22] K. Boodhoo, Spinning disc reactor for green processing and synthesis, Ch. 3, in: K. V.K. Boodhoo, A.P. Harvey (Eds.), Process Intensification for Green Chemistry: Engineering Solutions for Sustainable Chemical Processing, Wiley-Blackwell, Oxford, 2013.
[23] R.J.J. Jachuck, C. Ramshaw, Process intensification: heat transfer characteristics of tailored rotating surfaces, Heat Recovery Sys. CHP 14 (5) (1994) 475–491.
[24] A. Aoune, C. Ramshaw, Process intensification: heat and mass transfer characteristics of liquid films on rotating discs, Int. J. Heat. Mass Transf. 42 (14) (1999) 2543–2556.
[25] O.K. Matar, G.M. Sisoev, C.J. Lawrence, Evolution scales for wave regimes in liquid film flow over a spinning disc, Physics of Fluids 16 (2004) 1532–1545.
[26] S. Mohammadi, A. Harvey, K.V. Boodhoo, Synthesis of TiO2 nanoparticles in a spinning disc reactor, Chem. Eng. J. 258 (2014) 171–184.
[27] S. Sana, K. Boodhoo, V. Zivkovic, Production of starch nanoparticles through solvent-antisolvent precipitation in a spinning disc reactor, Green Proces. Synthe. 8 (1) (2019) 507–515.
[28] B. De Caprariis, M. Di Rita, M. Stoller, N. Verdone, A. Chianese, Reaction-precipitation by a spinning disc reactor: influence of hydrodynamics on nanoparticles production, Chem. Eng. Sci. 76 (2012) 73–80.
[29] W.R. Rathod, V.K. Rathod, Continuous preparation of nimesulide nanoparticles by liquid antisolvent precipitation using spinning disc reactor, J. Chem. Technol. Biotechnol. 94 (3) (2019) 919–926.
[30] N. Jeremic, Solvent removal from polymer dispersion using SDR technology, University of Newcastle upon Tyne, 2005.
[31] D. Ghiasy, M.T. Tham, K.V. Boodhoo, Control of a spinning disc reactor: an experimental study, Ind. Eng. Chem. Res. 52 (47) (2013) 16832–16841.
[32] A. Adamu, F.R. Abegão, K. Boodhoo, Solvent-free synthesis of nanostructured TiO2 in a continuous flow spinning disc reactor for application to photocatalytic reduction of CO2, Tetrahedron Green Chem 1 (2023) 100007.
[33] K.V. Boodhoo, S.R. Al-Hengari, Micromixing characteristics in a small-scale spinning disk reactor, Chem. Eng. Technol. 35 (7) (2012) 1229–1237.
[34] G.E. Acquah, B.K. Via, O.O. Fasina, L.G. Eckhardt, Rapid quantitative analysis of forest biomass using fourier transform infrared spectroscopy and partial least squares regression, J. Anal. Methods Chem. 2016 (2016).
[35] Y. Lu, Y.C. Lu, H.Q. Hu, F.J. Xie, X.Y. Wei, X. Fan, Structural characterization of lignin and its degradation products with spectroscopic methods, J. Spectroscopy 2017 (2017).

[36] T. Rashid, C.F. Kait, T. Murugesan, A "Fourier Transformed infrared" compound study of lignin recovered from a formic acid process, Procedia Eng. 148 (2016) 1312–1319.
[37] Faix, O., 1992. Fourier transform infrared spectroscopy, Ch. 4 in methods in lignin chemistry (pp. 83–109). (Eds Stephen Y. Lin and Carlton W. Dence Springer), Berlin, Heidelberg.
[38] G.S. Müller, FTIR-ATR spectroscopic and FTIR-FPA microscopic investigations on panel board production processes using grand fir (Abies Grandis (Douglas Ex D. Don) Lindl.) and European beech (Fagus Sylvatica L.), Georg-August University of Göttingen, 2008.
[39] J. Bouajila, P. Dole, C. Joly, A. Limare, Some laws of a lignin plasticization, J. Appl. Polym. Sci. 102 (2) (2006) 1445–1451.
[40] A. Nada, H. Abou Yousef, S. El-Gohary, Thermal degradation of hydrolyzed and oxidized lignins, J. Therm. Anal. Calorim. 68 (1) (2002) 265–273.
[41] S. Sana, V. Zivkovic, K. Boodhoo, Shear-thinning effect of the spinning disc mixer on starch nanoparticle precipitation, Processes 8 (12) (2020) 1622.
[42] Quarterly Energy Prices UK July to September 2022 and Estimates For 2022, Department for business, energy & industrial strategy, 2022. Available at, https://assets.publishing.service.gov.uk/government/uploads/system/uploads/attachment_data/file/1126144/quarterly-energy-prices-december-2022.pdf. Accessed: 19/03/23.
[43] P. Oxley, C. Brechtelsbauer, F. Ricard, N. Lewis, C. Ramshaw, Evaluation of spinning disk reactor technology for the manufacture of pharmaceuticals, Ind. Eng. Chem. Res. 39 (7) (2000) 2175–2182.
[44] P. Schulze, Lignin separation from ethanol water pulping liquors, Otto-von-Guericke-Universität, Magdeburg, 2018.
[45] X. Liang, J. Liu, Y. Fu, J. Chang, Influence of anti-solvents on lignin fractionation of eucalyptus globulus via green solvent system pretreatment, Sep. Purif. Technol. 163 (2016) 258–266.
[46] P.P. Thoresen, L. Matsakas, U. Rova, P. Christakopoulos, Recent advances in organosolv fractionation: towards biomass fractionation technology of the future, Bioresour. Technol. 306 (2020) 123189.
[47] T. Carr, K. Boodhoo, F. Russo Abegao, Valorisation of hemicellulose by-products via antisolvent precipitation in a spinning disc reactor, in: 31st European Biomass Conference & Exhibition, Bologna, Italy, 2023.
[48] S. Jahnke, K. Jasch, S. Scholl, Wiped film evaporators: segmental assessment of wetting behavior and heat transfer performance, Chemical Eng. Res. Design 163 (2020) 67–75.
[49] J. Song, W. Tian, X. Xu, Y. Wang, Z. Li, Thermal performance of a novel ultrasonic evaporator based on machine learning algorithms, Appl. Therm. Eng. 148 (2019) 438–446.
[50] K. Huang, Y. Hu, X. Deng, Experimental study on heat and mass transfer of falling liquid films in converging-diverging tubes with water, Int. J. Heat Mass Transf. 126 (2018) 721–729.
[51] J.S. Prost, M.T. Gonzalez, M.J. Urbicain, Determination and correlation of heat transfer coefficients in a falling film evaporator, J. Food Eng. 73 (4) (2006) 320–326.